Opto-Electronic Science

Supplementary information

March 2025, Vol. 4, No. 3

DOI: 10.29026/oes.2025.240022 CSTR: 32246.14.oes.2025.240022

Design, setup, and facilitation of the speckle structured illumination endoscopic system

Elizabeth Abraham and Zhaowei Liu*

Department of Electrical and Computer Engineering, University of California, San Diego, 9500 Gilman Drive, La Jolla, California 92093, United States.

*Correspondence: ZW Liu, E-mail: zhaowei@ucsd.edu

This file includes:

Supplementary information for this paper is available at https://doi.org/10.29026/oes.2025.240022

Section 1: Schematic of winding mechanism

In Fig. S1, the heat shrink is secured at two different locations: one on the head of the endoscope where the sleeve sits, and the other at the end of the inserted portion of the body of the endoscope. Medical or film tape, along with the external medical tubing, is additionally used to secure the fiber at fixed lengths of about 10 centimeters so as not to have large portions of the fiber sagging. The medical TPU (thermoplastic polyurethane) tubing bound around the scope is roughly ~1 millimeter wider than the body of the scope to help provide space to accommodate the extra lengths of the MM fibers, which may be beneficial, particularly when the endoscope bends at small angles during navigation. Table S1 indicates the bend radius leverage of the MM fiber with the endoscope.

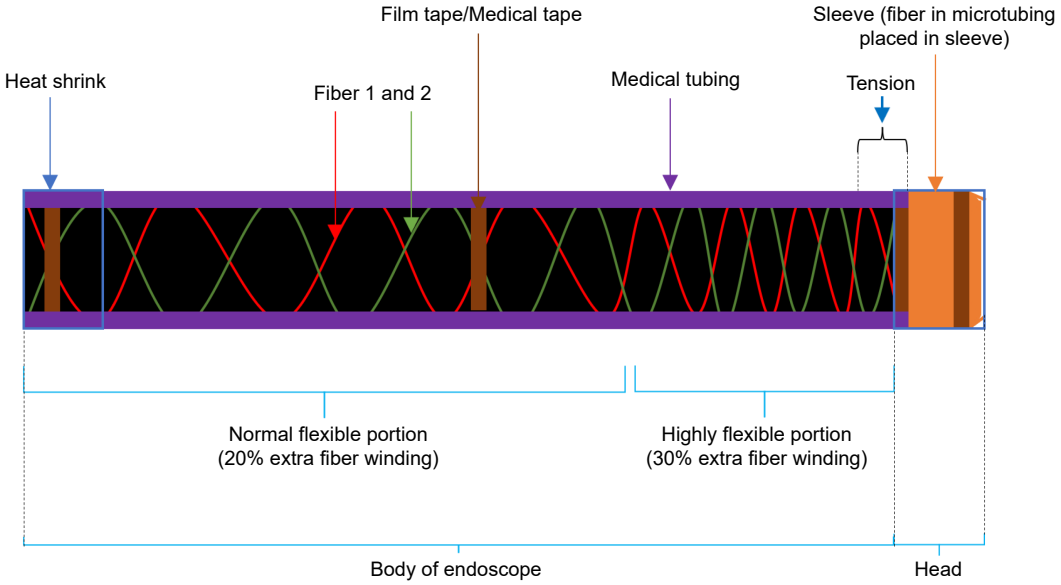

Fig. S1 | The MM fibers winding around the endoscope.

Table S1 | Bend radius leverage.

Bending length	Endoscope	MM fiber	Bending leverage of the endoscope (flexibility w/o breakage)
Long term bend radius	7 cm	3 cm	~ 57%
Short term bend radius	5 cm	1.5 cm	~ 70%

Even though we observe from Table S1 that the flexibility without breakage of MM fiber when the endoscope's highly flexible portion undergoes rigorous navigation is between 57%–70%, which is a good estimate, there occurs tension between the rigid head portion of the endoscope where the MM fiber is firmly bound and the flexible portion where the MM fiber is moderately bound, as indicated in Fig. S1. To alleviate this and the possibility of torque transmission, the highly flexible portion of the endoscope, which is typically around 8 cm in length, is where 30% of extra MM fiber is moderately wound for unhindered movement of the endoscope and potentially preventing breakage of the fiber during such dynamic movements (Fig. S1). For the remainder of the length of the endoscope, which remains reasonably flexible, 20% of extra fiber is moderately wound around the rest of the body of the endoscope. The 20% to 30% of extra MM fiber is chosen by test and by examining the freefall bend radius of the endoscopic probe. Since the endoscope has lock knobs present capable of locking the scope at different positions, once the ideal angle and position of imaging is identified, the scope can be locked in place securely allowing for controlled precision in imaging and measurement.

Section 2: Thickness metrics, the add-on specifications and sterilization

Table S2 | Thickness metrics of the prototype.

Components	Laboratory prototype thickness	Projected clinical prototype thickness
Resin (sleeve)	Grey pro (0.7 mm) (head)	No matter the resin material, it would be better to maintain the 0.7 mm thickness for structural integrity (head)
Fiber	0.25 mm (placed in the add-on slots: does not count to thickness metrics) (head + body)	0.25 mm (placed in the sleeve slots: does not count) (head + body)
Film tape	Polyamide (0.1 mm) (head + body)	Medical grade film (polyethylene with medical grade acrylic adhesive: fluid resistant) - 0.12 mm (head +body) Acrylic adhesives binds well both to resin (head) and TPU materials (endoscope body)
Adhesive (for fiber or others)	Cyanoacrylate adhesive (Henkel: Loctite 4851 or Gorilla 2-part epoxy) (~ < 0.15 mm: head) Cyanoacrylate adhesives bond well with silica (fiber) and resin material - grey pro (sleeve)	Adhesive is determined primarily by the type of resin used Medical grade silicon-based adhesives would bind to the microtubing (silicone) and the resin material (sleeve) (head) (~ < 0.15 mm)
Medical film / Tubing	Polyether TPU (0.08 mm) (body)	Polyether TPU (0.08 mm) (body)
Microtubing (silicone)	0.6 mm (OD) (placed in the fiber slot - head)	0.6 mm (OD) (placed in the fiber slot: does not count: head)
Heat shrink	Polyolefin: 0.4 mm (thickness after shrink) (head + body)	0.4 mm (thickness after shrink) (head + body) This is the same material under the group of polymers that are typically used for making endoscopes
PDMS	N/A	Does not contribute to the overall thickness as it is placed laterally
Overall thickness (add-on with 3D printed resin-based sleeve)	Head: 1.4 mm (2.8 mm, considering both up and down sides of the endoscope) Body: 0.8 mm (2.6 mm − (1.6 mm + 1 mm (TPU film excess space)), considering both up and down sides of the endoscope)	Head: 1.42 mm (2.84 mm, considering both up and down sides of the endoscope) Body: 0.82 mm (2.64 mm − (1.64 mm + 1 mm (TPU film excess space)), considering both up and down sides of the endoscope)
Overall thickness (add-on with sleeve made from ultra-thin glass)	N/A	Head: 1.12 mm (2.24 mm, considering both up and down sides of the endoscope) (with 300mm wall thickness) Body: 0.82 mm (2.64 mm − 1.64 mm + 1 mm, TPU film excess space), considering both up and down sides of the endoscope)

N/A: Not applicable

Using the add-on, the movement leverage of the SSIE endoscopic add-on is explored in Table S3.

Table S3 | Overall thickness metrics and movement leverage of the add-on.

Endoscope regions	Overall thickness and movement flexibility
Endoscopic head with add-on (rigid portion)	2.84 mm (3D printed resin) 2.24 mm (glass-based sleeve)
Endoscope body with add-on (flexible portion)	2.64 mm
Esophagus / colon	2 cm (minimum) – 8 cm (maximum)
WLE (endoscope) diameter (head and body)	<1.32cm (at maximum)
Endoscope with add-on (head / rigid portion)	~ 1.60 cm (3D printed resin) ~ 1.54 cm (glass-based sleeve)
Endoscope with add-on (body / flexible portion)	~1.58 cm
Movement leverage of endoscope (with 3D printed resin)	~20% – 21% (head / body – minimum) ~80% (head / body – maximum)
Movement leverage of endoscope (with glass)	~ 21% – 23 % (head / body – minimum) ~ 80% – 81% (head / body – maximum)

Using high precision stereolithographic (SLA) 3D printing with smaller nozzle sizes of 0.2 millimeters, a minimum wall thickness of 0.2 millimeters can be achieved[S1,S2]. However, lowering wall thickness to such fine limits may compromise the sleeve's structural integrity, considering the MM fiber thickness ranging above 0.2 millimeters. The diameters of endoscopes and colonoscopes typically range from 10–13.2 millimeters. The diameters of the colon and esophagus are between 2 to 8 centimeters, which are well above the standard white light endoscopic and colonoscopic instrument diameters. The objective of the fabricated add-on's overall thickness (outer diameter, OD) is not to exceed a few millimeters, considering both sides (top and bottom) of an endoscope (Fig. 2(f, g) in the main text), to ensure safe navigation of the endoscopic probe within the human body for future clinical systems (Tables S2 and S3).

To fasten the MM fiber, cyanoacrylate adhesive is used to securely bind the MM fiber to the add-on made of resin material. For clinical translation, a biocompatible medical-grade cyanoacrylate suitable for clinical usage can be adopted[S3]. Moreover, medical films with adhesives or film tapes, as shown in Fig. 2(f) in the main text, can also be used to secure the fibers on both the head (rigid portion) and the body (flexible portion) of the endoscope instead of cyanoacrylate adhesive. The film tape is additionally utilized to secure the fibers at fixed locations throughout the endoscopic probe (Fig. 2(f), main text). As the thickness of the film tapes is highly minimal, typically around a tenth of a millimeter, it would not significantly add to the overall thickness of the add-on and the rest of the endoscope (Tables 3 and 4). To keep the compact materials around the scope in place, heat sealing may not be the best option for clinical translation, as there is a potential for the TPU film to have rugged edges when subjected to heat sealing. Custom-made TPU film that fits the probe's diameter, as used in this study (Fig. 2(g) in the main text), would be the best way to avoid any possible rugged edges and to ensure safe navigation of the endoscope within the human body.

Furthermore, even with the incorporation of the add-on for medical devices, standard sterilization protocols are commonly practiced to ensure cleanliness and safety of the device. Under the umbrella of sterilization protocols, ethylene oxide sterilization (EtO) is the most commonly used approach in GI endoscopy[S3–S7]. Since ethylene oxide is highly compatible with most polymers and plastics, using it on polyether TPU (film), polyolefin (heat shrink), optical fibers (silica), and resins (sleeve) should not be a cause of concern[S8,S9]. The EtO process does not cause chemical degradation of silica or polymer-based materials[S8,S9]. Therefore, employing EtO sterilization for the add-on may not compromise its physical integrity or the optical properties of the system, despite the fact that the fiber core is additionally well protected by its cladding (fluorine-doped silica). The same analogy can be drawn to high level disinfectants also used in endoscopic sterilization. It is observed that these disinfectants whether Cidex or ortho-phthaladehyde, is found to be successfully tested on medical devices including polymers and plastics, hence, such protocols should not be a cause of concern for the prototype explored[S10–S12]. However, there may be some potential long-term effects, such as surface-based embrittlement of resins and polymers, when multiple cycles of ethylene oxide sterilization are used[S13]. If such embrittlement arises, the add-on and each of its integral components are readily replaceable given their cost-effectiveness. Since the components used in the add-on are EtO sterilization tolerant, the add-on can be disinfected and reused. Nonetheless, the fiber tips may wear out over time with usage and may need to be clipped. However, this is a straightforward and relatively inexpensive operation.

Section 3: Add-on sleeve with microtubing

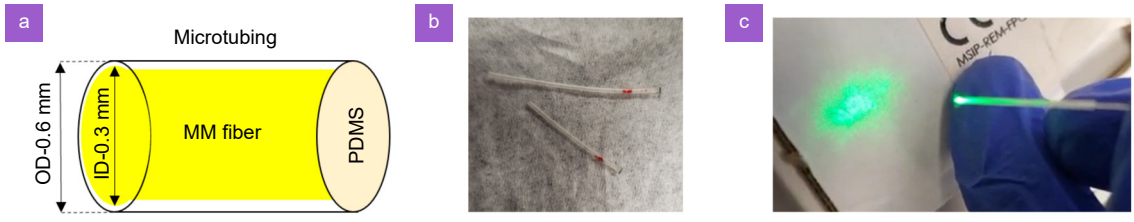

Fig. S2 | Microtubing for a clinical based SSIE system. (**a**) The schematic of the microtubing with the MM fiber. (**b**) Picture of the two microtubing sealed with PDMS to be placed on either end of the endoscope. (**c**) Picture of the transmission of specular illumination from the MM fiber through the microtubing sealed with PDMS.

The microtubing diameters are chosen to accommodate the multimode fibers, which have a diameter of 0.25 mm (250 μm). The right end of the tubing is sealed with polydimethylsiloxane (PDMS) (Fig. S2(b)). PDMS is chosen as a sealant because of its high optical transparency, chemical inertness in aqueous environments, and biocompatibility[S14,S15]. The nature of the microtubing protects the optical fiber from the external body environment. PDMS manufactured through conventional procedures produces flat surfaces, and grinding and lapping are common practices that are useful for achieving even illumination on the sample[S16–S18]. Considering the refractive index of PDMS, which is 1.43, and applying Snell's law, $\theta 1$ and $\theta 4$ (Fig. S3) would theoretically be equal.

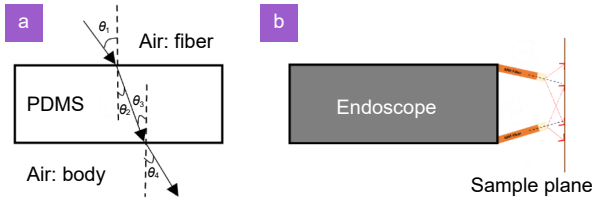

Fig. S3 | (**a**) The interface medium between fiber and body with angles of incidence and refractions. (**b**) Cross sectional view of the endoscope with the fiber (orange, placed inside the microtubing) and PDMS(yellow tips) showing a few illumination paths. Note, the fiber is presented to be slightly protruding to convey the above message and for schematic purposes.

The microtubing and the PDMS are placed within the ridges of the two-sided groove on the outer sleeve (Fig. 3(c, d) in the main text), well protected within the heat shrink around it, leaving no portions of the microtubing or the PDMS exposed to the external environment. Since the fiber is placed on a tilted slope of the sleeve, smaller tilts are preferred for shorter working distance (WD), as in Section 4. Even the largest angle of incidence and illumination dispersion (θ_1 and θ_4) will still allow a reasonable amount of illumination light to reach the sample, which is sufficient for imaging, as shown in Fig. S3(b). If the illumination intensity is low due to large angles of dispersion, the laser illumination intensity can be increased to meet the illumination needs. However, care must be taken to maintain the laser power density within safe limits permitted for use in the human body. Previous studies have shown the use of a laser power density of 20 mW/cm^2 at the corneal plane of the human eye[S19,S20]. In comparison, the SSIE technique would require only a few milliwatts of laser power (about 1–2 mW) to collect sample frames. Regarding the thickness of the PDMS, PDMS films can be manufactured to be very thin, down to a few hundred nanometers[S21]. However, from a realistic perspective, a thickness of a few millimeters is considered safe for its transfer and adhesion onto the silicone microtubing (Fig. S2(b, c)). To facilitate this, a film of a specific thickness, the same as the desired PDMS thickness, can be chosen as the spacer between the two plates[S18]. Additionally, the PDMS seal also protects the human body against the exposed fiber tip. If the PDMS becomes blocked by body fluid or solid molecules, a water jet, typically used to wash away blood, mucosa, or other substances from the tip of the endoscope, can be used[S22].

Since the microtubing has a diameter of about 0.6 mm (OD), the diameter of the fiber slot (Fig. 2(a, b), main text) is designed to be 700 microns (0.7 mm) in wall thickness. This design allows for the potential accommodation of the fiber slot with the microtubing and prevents any potential cracks from appearing on the add-on when the endoscope maneuvers under tension in a clinical model. The chosen microtubing is made of silicone material, which is selected not only for its medical biocompatibility but also for its ability to withstand standard medical sterilization protocols. Silicone is bio-durable, temperature-resistant, and chemically inert[S23–S26]. To bind the polydimethylsiloxane (PDMS) to the silicone tubing, microscopic amounts of biocompatible adhesives can be used between the two surfaces of the microtubing and the PDMS (Fig. S2(b, c)). Biocompatible epoxy or silicon-based adhesives can be used for this purpose[S27,S28]. The silicone-based adhesives can also be spin-coated on the silicon tubing to achieve a thickness of a few microns[S27]. If needed, the bonding quality between the two surfaces can be further enhanced by combining the adhesive-based mechanism with other suitable binding approaches[S27]. During the adhesion process, the silicone tubing can be securely held using jaw-styled tubing clamps or keck ramp clamps. After applying the silicone adhesive onto the tubing or spin coating it, the PDMS film is mounted onto the silicon tubing. Through the other end of the silicone tubing, the multimode fiber is inserted, and the fiber tips are clipped using the standard fiber stripping tool for the FG050UGA multimode fiber.

A detailed study of this adhesion process and the production of PDMS will be explored for the clinical implementa-

tion of the Speckle structured illumination endoscopy (SSIE) system in the near future. The materials and components used in the design are easily accessible, simple to assemble, and readily available, making it an ideal design and system for practical use. The add-on in this study was assessed on two endoscopic systems with different structural geometries, namely the Teslong's and the CV-160 system. The design sleeve fitted well on both systems by adjusting the design parameters of the computer-aided design (CAD), primarily incorporating the outer diameter and length (L) of the add-on. Another possible model for the clinical adaptation of the SSIE design involves replacing the current resin add-on with custom-manufactured ultra-thin glass. Ultra-thin glass can be manufactured with a thickness of up to 25 microns. However, since the fiber has a thickness of 250 microns, the minimum thickness of the ultra-thin glass material for the add-on needs to be greater than 250 microns. A comparison based on thickness is provided in Table S2, and Section 3. Additionally, custom manufacturing the sleeve using glass will eliminate the possibility of rugged surfaces, reducing the likelihood of uneven optical illumination.

Section 4: Tilt angle vs working distance

Considering the CV-160 system, which has a diameter of 1.2 cm, the generated schematic below (Fig. S4) illustrates the setup. In a realistic White Light Endoscopy (WLE) system, working distances typically range from 0.5 cm to approximately 10 cm. Based on Fig. S2, we observe that tilt angles (θ) between 40° to 89° are suitable for working distances ranging from 0.5 cm to 8.6 cm. This indicates that even for a small working distance of 0.5 cm, a tilt angle of approximately 40° is preferred. This tilt angle is not considered a narrow bend and facilitates the securement of the multimode (MM) fiber onto the sleeve. However, tilt angles greater than 90° are practically not possible in the arrangement of the MM fiber on the add-on (Fig. 2(a, b), main text). Tilt angles exceeding 90° would cause the specular illumination from the fibers to point away from the sample, which goes against the objective of the study. Therefore, tilt angles greater than 90° are not explored. To ensure safety, the end of the add-on where the tilt angle is located, as well as its corresponding slope, are extra beveled in the CAD design. This design feature prevents the presence of rough corners that could potentially scratch the MM fibers attached to it (Fig. 2(a, b), main text). From Fig. S4, even for short working distances of 2.7 cm, a tilt angle (θ) of 77.5° is required. Although this may not be classified as a sharp angle, which ideally would be only a few° (<10°), the relatively large tilt of the slope in the design itself (which is extra beveled) does not compromise the placement and structural integrity of the MM fibers. Additionally, the external cladding of the MM fibers provides excellent cover and protection for the fiber core.

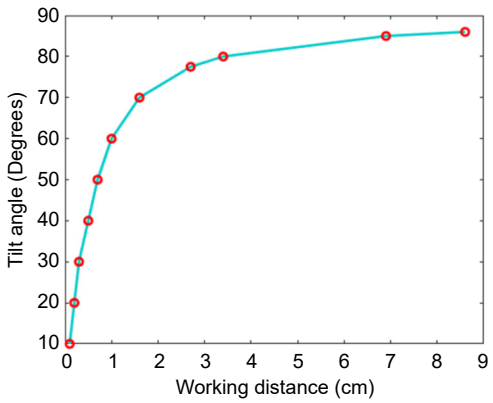

Fig. S4 | Plot of tilt angle of the MM fiber vs working distance

Section 5: Colon phantom construction

This section addresses the construction of a colon phantom model used for imaging. The phantom is created using a silicone composite pad that replicates the anatomical structure of human tissues. It consists of three tissue layers: the epidermis, dermis, and subcutaneous tissue. The inclusion of mesh layers in the silicone pad protects it against potential rips, wear, and tear. These composite pads, made of silicone, are highly resistant and flexible, similar to dragon skin.

Dragon skin, also made of silicone, is commonly used for constructing human body phantoms[S29,S30]. To enhance realism, the phantom model incorporates simulated polyp growths, bumps, and crevices (Fig. 2(c, d), main text). Acrylic rigid clear tubes and couplers are utilized to construct the overall external structure of the human colon (Fig. 2(e), main text). The couplers serve as bridges between the acrylic tubes but are not integrated with the silicone itself. The silicone within the acrylic tubes mimics human tissue surfaces and serves as the imaging target. In this study, small amounts of rhodamine dye, a fluorescent agent, are applied to the tissue surface of the composite pads prior to imaging. Images are captured by placing the distal tip of the endoscope at various imaging distances from the surface of the silicone pads. The fluorescent agent allows for the creation of features on the phantom through drop-casting (Fig. 2(a), main text). Additionally, fine needles are used to draw features on the phantom to simulate blood vessels (Fig. 2(b), main text). The fluorescent light reflected from the sample is directed into the endoscopic charged coupled device (CCD). The acquired images are then analyzed and processed on a personal computer.

Section 6: Generic comparison of high-resolution endoscopic methods vs the SSIE

Table S4 | Generic comparison between different methods.

Specifications	Field of View	Resolution	Depth of Field	Maximum Number of Uses
WLE (Any modality*)	90°–170°	Diffraction limit of the system	1.5−100 mm	Can be reused
CLE	240−600 μm	Diffraction limit of the system	40−250 μm	10-20 (probe-based systems)
EC	120−400 μm	Diffraction limit of the system	50 μm	10−20 (probe-based systems)
OCT	1 mm−1 cm	Diffraction limit of the system	2.8−5 mm	Can be reused
HRME	720 μm	Diffraction limit of the system	250−500 μm	Can be reused
HRE	120°−140°	Diffraction limit of the system	N/A	Can be reused
FBM	250 μm	Diffraction limit of the system	N/A	Can be reused
SSIE	As large as that a WLE may allow	2−4.5 times the diffraction limit of the system the add-on is incorporated onto	As large as that of WLE may allow	Can be reused

N/A: Not available * High definition or otherwise[S31−S33]

The SSIE method shows potential for improvement in terms of resolution, depth of field (DOF), and field of view (FOV) compared to other high-resolution techniques, as shown in Table S4. From Table S4, it can be observed that the SSIE offers much larger FOV and DOF compared to techniques such as Confocal Laser Endomicroscopy (CLE), Electronic Chromoendoscopy (EC), high-resolution Optical Coherence Tomography (OCT), High-Resolution Microendoscopy (HRME), and Fibered Confocal Fluorescence Microscopy (FBM). The FOV of SSIE extends approximately (17-60) times and the DOF extends around (10–100) times compared to the other methods at its best. The objective of SSIE is to provide high-resolution imaging with wide FOV and large DOF, resulting in faster surface screening and visualization of the sample compared to other state-of-the-art (SOA) techniques. Addressing the metrics of resolution, FOV, and DOF collectively is not commonly observed in the latest high-resolution modalities, except in traditional OCT systems. However, OCT also has its limitations. Although OCT is a powerful imaging method that allows for wide FOV and DOF, the advantages of SSIE lie not only in achieving optimal imaging metrics but also in its ease of translation due to minimal hardware modifications, cost-effectiveness, and reduced learning curve. The learning curve and specific applicability of OCT among gastroenterologists may be impacted by its low translatability, which has been a problem in recent times even in areas where the systems can be afforded[S34−S44].

In our future studies, a clinical trial will be conducted to investigate the impact of Speckle structured illumination Endoscopy (SSIE) and interobserver reproducibility for validation in a clinical setting. Achieving cellular-level resolution with the standard White Light Endoscopy (WLE) system used in this study may exceed the current system's capabilities. However, resolution can be further improved by reducing the working distance (WD)[S21]. Moreover, this limitation is not significant since the concept of SSIE as an add-on can be applied to the latest state-of-the-art (SOA) high-resolution endoscopes, supplementing, and surpassing the diffraction limits of those systems at wide FOV and DOF. By combining the current high-resolution fluorescent imaging SSIE system with other molecular-specific techniques, such as opti-

cal contrast agents targeted to epithelial biomarkers, the specificity and sensitivity of the technology can be enhanced. In this study, rhodamine fluorescent dye was used for laboratory imaging demonstration on the colon phantom. However, for a clinical system, the selection of a bright, selective fluorescent dye is essential to achieve a good frame rate and image quality. Acriflavine hydrochloride, a fluorescent dye commonly used in imaging studies of the gastrointestinal (GI) epithelium and other studies, has shown promising results without any reported adverse effects. It may prove useful for the clinical implementation of the SSIE system[S45–S49]. Furthermore, the imaging procedure of SSIE does not involve optical sectioning and does not require the rejection of fluorescent light, as in a confocal system. Therefore, specific superficial imaging and labeling techniques may further improve image detail.

Section 7: Incorporation of the optical filter in the sleeve add-on for a portable system

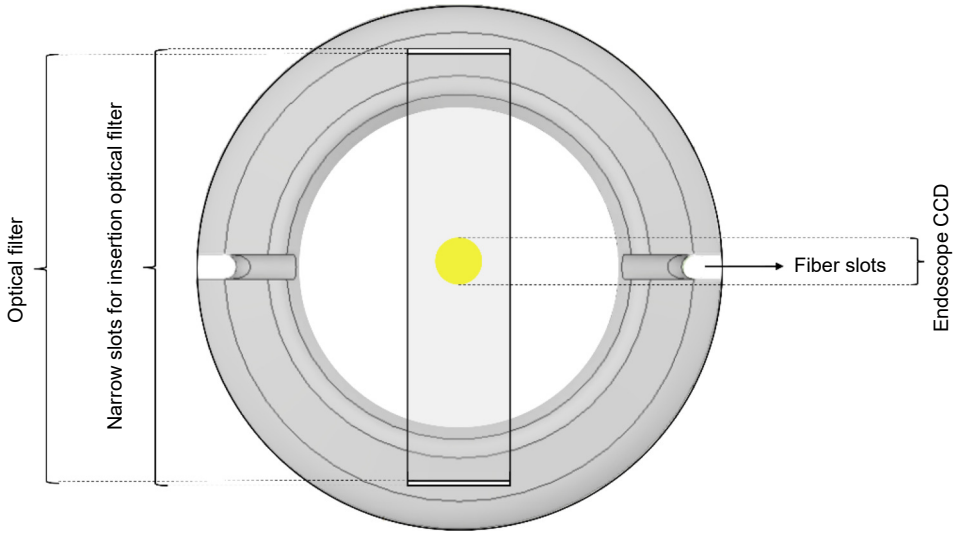

Fig. S5 | The frontal cross section with ultra-thin optical filters placed in narrow slits on the endoscopic sleeve add-on

The optical filter shown in Fig. S5 serves as a replacement for the physical filter used in the SSIE study, as demonstrated in the main section, for a portable futuristic clinical SSIE system. The thickness of the optical filters used in Fig. S5located at either end of the add-on, is approximately a few hundred microns thick (~100–500 μm). Therefore, the rectangular slots would ideally have dimensions within this range[S50]. These rectangular slits are positioned in the vertical arm, as illustrated in Fig. S5, away from the area where the fibers are placed. The sloping portion of the external sleeve is about 300 microns thicker than the walls of the sleeve, with a total thickness of 700 microns, to support the placement of the multimode (MM) fibers. The optical filter slits are cut into this sloping portion of the sleeve, and they are approximately 100–500 microns wide horizontally and 1000 microns thick vertically to accommodate the dimensions of the ultra-thin optical filters. The slits are placed as close as possible to the endoscopic charged coupled device (CCD). Ideally, the slots would be located exactly as depicted in Fig. S6.

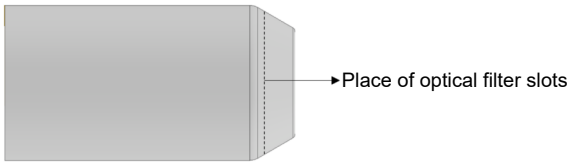

Fig. S6 | The side view of the sleeve add-on indicating the placement of the rectangular slits.

The ultra-thin optical filters, primarily composed of polymers and occasionally plastic in rare cases, can be attached to the rectangular slits using polymer-to-resin biocompatible adhesives. Polymers are preferred as they are biocompatible and biodegradable. Moreover, the dimensions of the rectangular slits can be adjusted to match the width of the en-

doscopic CCD in order to avoid obstructing other endoscopic channels such as air, water, light, and biopsy channels. These channels are typically placed laterally from the CCD to ensure they do not interfere with its operation, offering an advantage for the placement of the optical filters (Fig. S5, S6). Therefore, the vertical positioning of the optical filters will not hinder or block other endoscope channels due to their lateral placement from the CCD. Additionally, the proximity of the slots to the CCD not only helps in reducing the working distance (WD) for imaging but also enhances the structural integrity of the add-on. The slope of the add-on acts as an additional barrier to the optical filters inserted in the slots, even though the filters are securely fixed to the sleeve using suitable adhesives. Since the optical filters are firmly attached on both ends to the external sleeve, there are no concerns regarding their potential disengagement. The implementation of this design will be further investigated in future clinical trials.

Section 8: Detection NA of Olympus CV-160 system vs Teslong's endoscope

In Fig. S7, it can be observed that the Teslong system's detection numerical aperture (NA) is measured to be twice as high as the CV 160 system at 1.5 cm, and extrapolated to be 2.7 times higher at 2.5 cm. A higher detection NA indicates better resolution in the images captured by the endoscope system. The frames from the CV-160 system is captured with the Ephiphan frame grabber that is connected to the processor of the 160 system via the VGA2USB port. Additionally, the CV-160 system, being an older model in terms of hardware and CCD capabilities, produces very poor-quality images that are heavily pixelated. Consequently, it was unable to capture any legible images with analytical capability. This limitation led to the utilization of the Teslong endoscope system in the imaging demonstrations for this study, which offers superior detection and hardware capabilities. By employing the Teslong system, the objective of the SSIE study is achieved by surpassing the diffraction limits of the endoscopic system, enabling high-resolution imaging with a wide field of view (FOV) and depth of field (DOF).

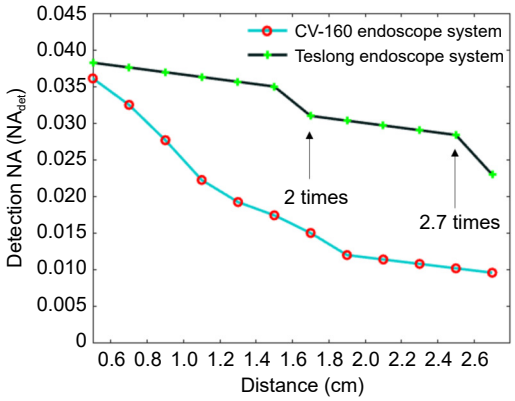

Fig. S7 | Plot of the CV 160 system vs the Teslong system. Plot of the detection NA of the two systems vs the imaging distance or WD of the endoscope. The blue curve represents the detection NA of the CV-160 endoscope system and the black curve represents the detection NA of the Teslong endoscope system.

Section 9: Qualitative image quality metrics

Table S5 | Perception based image quality metric score comparison.

Figures	Diffraction limited image	Enhanced image
Figure 5	91.3 (Fig. 5(a))	91.27 (Fig. 5(b))
	91.5 (Fig. 5(f))	87.9 (Fig. 5(g))
	77.1 (Fig. 5(j))	74.7 (Fig. 5(k))
	89.3 (Fig. 5(o))	84.8 (Fig. 5(p))
	80.1 (Fig. 5(s))	75.8 (Fig. 5(t))
Average	85.8	82.8
Figure 6 (5.7 cm)	78 (Fig. 6(a))	76.3 (Fig. 6(b))
		61.8 (Fig. 6(c))
		73.2 (Fig. 6(d))
		71.7 (Fig. 6(e))
		75.1 (Fig. 6(f))
		69.3 (Fig. 6(g))
		70 (Fig. 6(h))
Average	78	71
Figure 6 (4.7 cm)	92.1 (Fig. 6(j))	87.6 (Fig. 6(k))
		89.0 (Fig. 6(l))
		86.6 (Fig. 6(m))
		86.2 (Fig. 6(n))
		88.4 (Fig. 6(o))
		87.9 (Fig. 6(p))
		86.1 (Fig. 6(q))
		89 (Fig. 6(r))
Average	92.1	87.6

Table S6 | Naturalness image quality metric score comparison.

Figures	Diffraction limited image	Enhanced image
Figure 5	14.9 (Fig. 5(a))	11.4 (Fig. 5(b))
	18 (Fig. 5(f))	10.4 (Fig. 5(g))
	19 (Fig. 5(j))	18.2 (Fig. 5(k))
	18.9 (Fig. 5(o))	18.6 (Fig. 5(p))
	19 (Fig. 5(s))	18.8 (Fig. 5(t))
Average	17.9	15.4
Figure 6 (5.7 cm)	18.9 (Fig. 6(a))	18.7 (Fig. 6(b))
		18.8 (Fig. 6(c))
		18.7 (Fig. 6(d))
		18.6 (Fig. 6(e))
		18.7 (Fig. 6(f))
		18.5 (Fig. 6(g))
		18.8 (Fig. 6(h))
Average	18.9	18.6
Figure 6 (4.7 cm)	19 (Fig. 6(j))	18.8 (Fig. 6(k))
		18.9 (Fig. 6(l))
		18.6 (Fig. 6(m))
		18.5 (Fig. 6(n))
		18.6 (Fig. 6(o))
		18.6 (Fig. 6(p))
		18.5 (Fig. 6(q))
		18.7 (Fig. 6(r))
Average	19	18.6

The lower the score of PIQE, NIQE in the enhanced frames, lower is the image distortion, noise and artifacts due image enhancement and higher is its perceptual image quality. The enhanced frames indicates a good perceptual and naturalness image quality individually and on average compared to the reference diffraction limited image as seen from Table S5, S6[S51,S52].

Section 10: Flow of the blind-SIM process in SSIE

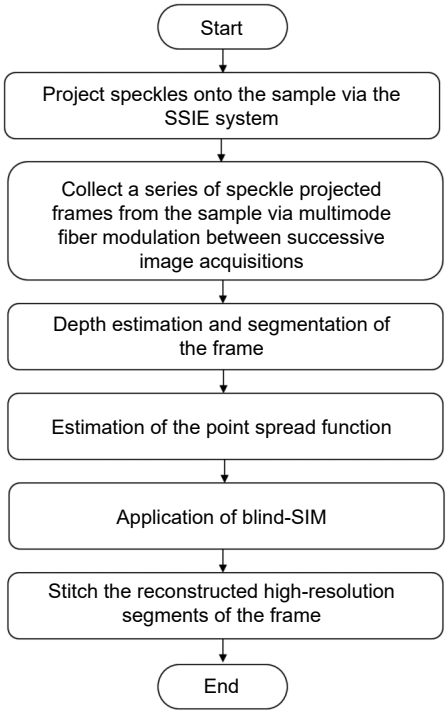

Fig. S8 | Flow chart of the blind-SIM process in SSIE

References

S1. Formlabs. Minimum wall thickness for 3D printing. Accessed 24 January 2023. https://formlabs.com/blog/minimum-wall-thickness-3d-printing.

S2. How to perfectly print a thin walled 3D print. Accessed 24 January 2023. https://dddrop.com/blog/how-to-perfectly-print-a-thin-walled-3d-print.

S3. Neto RTM, Mello I, da Silveira Moretti AB et al. In vivo qualitative analysis of the biocompatibility of different cyanoacrylate-based adhesives. *Braz Oral Res* **22**, 43–47 (2008).

S4. Jones A. Study: vaporized peroxide sterilization method damages GI endoscopes. Accessed 24 January 2023. https://singleuseendoscopy.com/study-vaporized-peroxide-sterilization-method-damages-gi-endoscopes.

S5. Lichtenstein D, Alfa MJ. Cleaning and disinfecting gastrointestinal endoscopy equipment. In Chandrasekhara V, Elmunzer BJ, Khashab MA et al. *Clinical Gastrointestinal Endoscopy* 3rd ed 32–50. e5 (Elsevier, Amsterdam, 2019).

S6. AdvaMed. Ethylene oxide & sterilization. Accessed 24 January 2023. https://www.advamed.org/industry-updates/policy-issues/sterilization-ethylene-oxide.

S7. Medical Design Briefs. Sterilization, packaging, and materials: CRITICAL CONSIDERATIONS. Accessed 24 January 2023. https://www.medicaldesignbriefs.com/component/content/article/mdb/pub/features/articles/27480.

S8. Proper sterilization methods for medical grade thermoplastic polyurethane (TPU). Accessed 24 January 2023. https://www.lubrizol.com/-/media/Lubrizol/Health/Literature/Proper-Sterilization-Methods-for-Lubrizol-TPUs.pdf.

S9. Sterilization effects on key properties of optical fibers. Accessed 24 January 2023. https://www.ofsoptics.com/sterilization-effects-on-key-properties-of-optical-fibers.

S10. UNC Health Care. Infection control manual. Accessed 23 June 2024. https://spice.unc.edu/wp-content/uploads/2017/03/Endoscope-IC0019.pdf.

S11. CIDEX OPA. Technical information. Accessed 23 June 2024. https://www.asp.com/sites/default/files/pdf/CIDEX%20OPA%20Technical%20Info%20AP-2000304.pdf.

S12. Akamatsu T, Minemoto M, Uyeda M. Evaluation of the antimicrobial activity and materials compatibility of orthophthalaldehyde as a high-level disinfectant. *J Int Med Res* **33**, 178–187 (2005).
S13. Miranda I, Souza A, Sousa P et al. Properties and applications of PDMS for biomedical engineering: a review. *J Funct Biomater* **13**, 2 (2021).
S14. Sanchez LEA, Jun NZX, Fiocchi AA. Surface finishing of flat pieces when submitted to lapping kinematics on abrasive disc dressed under several overlap factors. *Precis Eng* **35**, 355–363 (2011).
S15. Horner N. Easy and inexpensive fabrication of PDMS films of different thicknesses. Accessed 24 January 2023. https://blogs.rsc.org/chipsandtips/2012/04/18/easy-and-inexpensive-fabrication-of-pdms-films-of-different-thicknesses/?doing_wp_cron=1673103831.0497310161590576171875.
S16. Weinhoffer E. The Whitworth three plates method. Accessed 24 January 2023. https://ericweinhoffer.com/blog/2017/7/30/the-Whitworth-three-plates-method?rq=The%20Whitworth%20Three%20Plates%20Method.
S17. Lee HD, Kim GH, Shin JG et al. Akinetic swept-source optical coherence tomography based on a pulse-modulated active mode locking fiber laser for human retinal imaging. *Sci Rep* **8**, 17660 (2018).
S18. Ávila FJ, Gambín A, Artal P et al. *In vivo* two-photon microscopy of the human eye. *Sci Rep* **9**, 10121 (2019).
S19. Kim D, Kim SH, Park JY. Floating-on-water fabrication method for thin polydimethylsiloxane membranes. *Polymers* **11**, 1264 (2019).
S20. Nakano T, Sato C, Sakurai T et al. Use of water jet instruments in gastrointestinal endoscopy. *World J Gastrointest Endosc* **8**, 122–127 (2016).
S21. Boudot C, Burkhardt S, Haerst M. Long-term stable modifications of silicone elastomer for improved hemocompatibility. *Curr Dir Biomed Eng* **2**, 21–25 (2016).
S22. Kimura M, Ishibashi K, Shibata A et al. A new decompression device for treating odontogenic cysts using a silicone tube. *Br J Oral Maxillofac Surg* **58**, 116–117 (2020).
S23. Curtis J, Colas A. Medical applications of silicones. In Ratner BD, Hoffman AS, Schoen FJ et al. *Biomaterials Science* 3rd ed 1106–1116 (Elsevier, Amsterdam, 2013).
S24. Vanguard. Medical grade silicone tubing. Accessed 24 January 2023. https://www.vanguardproducts.com/medical-grade-silicone-tubing.
S25. Borók A, Laboda K, Bonyár A. PDMS bonding technologies for microfluidic applications: a review. *Biosensors* **11**, 292 (2021).
S26. Rośkowicz M, Godzimirski J, Komorek A et al. The effect of adhesive layer thickness on joint static strength. *Materials* **14**, 1499 (2021).
S27. Zulina N, Caravaca O, Liao GQ et al. Colon phantoms with cancer lesions for endoscopic characterization with optical coherence tomography. *Biomed Opt Express* **12**, 955–968 (2021).
S28. Smith GT, Lurie KL, Zlatev DV et al. Multimodal 3D cancer-mimicking optical phantom. *Biomed Opt Express* **7**, 648–662 (2016).
S29. ASGE Technology Committee. Confocal laser endomicroscopy. *Gastrointest Endosc* **80**, 928–938 (2014).
S30. Engineering M. Report on emerging technology GI endoscopes. Accessed 24 January 2023. https://www.semanticscholar.org/paper/Report-on-Emerging-Technology-Gi-Endoscopes/d851b3d7b0ae90605e6df3439c5d8d73b52868b4.
S31. Wang QZ, Khanicheh A, Leiner D et al. Endoscope field of view measurement. *Biomed Opt Express* **8**, 1441–1454 (2017).
S32. Popescu DP, Choo-Smith LP, Flueraru C et al. Optical coherence tomography: fundamental principles, instrumental designs and biomedical applications. *Biophys Rev* **3**, 155 (2011).
S33. Kirsten L, Schindler M, Morgenstern J et al. Endoscopic optical coherence tomography with wide field-of-view for the morphological and functional assessment of the human tympanic membrane. *J Biomed Opt* **24**, 031017 (2018).
S34. Chopra R, Wagner SK, Keane PA. Optical coherence tomography in the 2020s—outside the eye clinic. *Eye* **35**, 236–243 (2021).
S35. Aumann S, Donner S, Fischer J et al. Optical coherence tomography (OCT): principle and technical realization. In Bille JF. *High Resolution Imaging in Microscopy and Ophthalmology* 59-85 (Springer, Cham, 2019).
S36. Burkhardt A, Walther J, Cimalla P et al. Endoscopic optical coherence tomography device for forward imaging with broad field of view. *J Biomed Opt* **17**, 071302 (2012).
S37. Gora MJ, Suter MJ, Tearney GJ et al. Endoscopic optical coherence tomography: technologies and clinical applications [Invited]. *Biomed Opt Express* **8**, 2405–2444 (2017).
S38. Schulz-Hildebrandt H, Pieper M, Stehmar C et al. Novel endoscope with increased depth of field for imaging human nasal tissue by microscopic optical coherence tomography. *Biomed Opt Express* **9**, 636–647 (2018).
S39. Cui DY, Chu KK, Yin BW et al. Flexible, high-resolution micro-optical coherence tomography endobronchial probe toward *in vivo* imaging of cilia. *Opt Lett* **42**, 867–870 (2017).
S40. Liu LB, Gardecki JA, Nadkarni SK et al. Imaging the subcellular structure of human coronary atherosclerosis using micro-optical coherence tomography. *Nat Med* **17**, 1010–1014 (2011).
S41. Kirtane TS, Wagh MS. Endoscopic optical coherence tomography (OCT): advances in gastrointestinal imaging. *Gastroenterol Res Pract* **2014**, 376367 (2014).
S42. Pittayanon R, Rerknimitr R. Role of digital chromoendoscopy and confocal laser endomicroscopy for gastric intestinal metaplasia and cancer surveillance. *World J Gastrointest Endosc* **4**, 472–478 (2012).
S43. Li H, Hou XH, Lin R et al. Advanced endoscopic methods in gastrointestinal diseases: a systematic review. *Quant Imaging Med Surg* **9**, 905–920 (2019).
S44. Hoffman A, Atreya R, Rath T et al. Use of fluorescent dyes in endoscopy and diagnostic investigation. *Visc Med* **36**, 95–103 (2020).
S45. Trivedi PJ, Braden B. Indications, stains and techniques in chromoendoscopy. *QJM* **106**, 117–131 (2013).

S46. Messmann H, Endlicher E, Freunek G et al. Fluorescence endoscopy for the detection of low and high grade dysplasia in ulcerative colitis using systemic or local 5-aminolaevulinic acid sensitisation. *Gut* **52**, 1003–1007 (2003).
S47. Fusco V, Ebert B, Weber-Eibel J et al. Cancer prevention in ulcerative colitis: long-term outcome following fluorescence-guided colonoscopy. *Inflamm Bowel Dis* **18**, 489–495 (2012).
S48. Polglase AL, McLaren WJ, Skinner SA et al. A fluorescence confocal endomicroscope for in vivo microscopy of the upper- and the lower-GI tract. *Gastrointest Endosc* **62**, 686–695 (2005).
S49. Kiesslich R, Burg J, Vieth M et al. Confocal laser endoscopy for diagnosing intraepithelial neoplasias and colorectal cancer in vivo. *Gastroenterology* **127**, 706–713 (2004).
S50. Edmund. What are ultra-thin filters. Accessed 24 January 2023. https://www.edmundoptics.com/knowledge-center/application-notes/optics/what-are-ultra-thin-filters.
S51. Venkatanath N, Praneeth D, Chandrasekhar Bh M et al. Blind image quality evaluation using perception based features. In *2015 Twenty First National Conference on Communications* 1–6 (IEEE, 2015); http://doi.org/10.1109/NCC.2015.7084843.
S52. Wu LY, Zhang XG, Chen H et al. VP-NIQE: an opinion-unaware visual perception natural image quality evaluator. *Neurocomputing* **463**, 17–28 (2021).